Optik - International Journal for Light and Electron Optics 271 (2022) 169879

Contents lists available at ScienceDirect

Optik

journal homepage: www.elsevier.com/locate/ijleo

The Brushless DC motor control system Based on neural network fuzzy PID control of power electronics technology

Ran Zhang *, Lianxue Gao

School of Electrical Engineering, Binzhou University, Binzhou, Shandong, 256600, China

ARTICLE INFO

Keywords:
Weights development
Power electronics
Neural network
Fuzzy PID control
Brushless DC motor
Control system
Technology emergence

ABSTRACT

In order to improve The Brushless DC motor control system Based on Particle Swarm Optimization Algorithm with Improved Inertia Weights development of power electronics technology emergence, The brushless director current (DC) motor is a new type of mechatronic motor that has been developed rapidly with the development of power electronics technology, The performance of the brushless DC motor control system, this paper starts with the brushless DC motor to improve the motor structure or use new materials. This paper uses the neural network fuzzy PID control method to carry out the study of the brushless DC motor control system, and chooses the correct control model and control target to solve the influence of the commutation process on the system. Moreover, this paper analyzes and designs the application of model prediction in BLDCM current loop control, and uses this control system to build a simulation model of brushless DC motor control system in MATLAB. The simulation results show that the brushless DC motor control system based on neural network fuzzy PID control can effectively improve the control effect.

1. Introduction

The brushless DC motor adopts the electronic commutation method in the working process, thus replacing the heavy mechanical commutation method of the traditional general DC motor. Since its working mode is very different from the brushed DC motor in the past, it is necessary to design a special control circuit to control its commutation. In recent decades, with the rapid development of electronic information power technology and high-power semiconductor switching components, brushless DC motors have gradually entered people's production activities. This type of motor has the characteristics of high power density, wide speed regulation range, high motor efficiency, small field weakening speed regulation range, fast dynamic response and small torque fluctuation. Therefore, it is widely used in CNC machining, servo drives, industrial robots and automotive electronics.

Compared with the traditional permanent magnet DC motor, the brushless DC motor not only has no mechanical brushes, but also interchanges the structure of the stator and the rotor. Its structure is completely opposite to that of the permanent magnet DC motor, that is, the rotor of the brushless DC motor is composed of permanent magnets, and the stator part is composed of iron core and armature winding. If the rotor of the motor is to work normally, some structural changes must be made. Otherwise, only the armature windings can generate a constant induced magnetic field after being energized, and the rotor cannot work normally. Therefore, an electronic commutation circuit must be added to complete the function of the mechanical commutation brush. The so-called electronic

* Corresponding author:
E-mail address: zhangran20pa@163.com (R. Zhang).

https://doi.org/10.1016/j.ijleo.2022.169879
Received 17 July 2022; Received in revised form 14 August 2022; Accepted 24 August 2022
Available online 28 August 2022
0030-4026/© 2022 Elsevier GmbH. All rights reserved.

commutation circuit is a circuit composed of a motor control circuit, a position sensing circuit and a power logic switch.

The brushless DC motor control system consists of three parts: motor, position sensor and switch circuit. The structure of the permanent magnet brushless DC motor is similar to that of the permanent magnet brushed DC motor, both of which establish a sufficient magnetic field in the motor air gap through the permanent magnet material, but the position of the permanent magnet material is different. The permanent magnet material of the permanent magnet brushed DC motor is on the motor stator, but the permanent magnet material of the permanent magnet brushless DC motor is on the rotor. The reason for this is that in order to generate continuous torque, the motor must commutate. The traditional permanent magnet brushed DC motor relies on the brush commutation device to change the direction of the electromagnetic field, which can only be achieved by changing the direction of the current, and the change of the current direction depends on the rotation of the rotor. At the same time, the magnetic field generated by the current on the rotor and the magnetic field generated by the permanent magnet material on the stator is jointly determined by the position of the brush commutation device and the rotation direction of the motor. However, in order to avoid the shortcomings of the brush commutation mechanism, the DC brushless motor relies on the position sensor and the switch circuit to commutate. The rotor is the moving part of the motor. In order to reduce the resistance during the movement, the physical connection with the outside world should be minimized, so the carbon brush on the traditional motor is removed and the magnetic field is generated by the permanent magnet. The position sensor is used to sense the position of the motor rotor relative to the stator, and the position sensor transmits the position of the rotor relative to the stator to the control circuit of the switch circuit with a certain code. The control circuit controls the on-off of the power switch according to certain control requirements and the drive logic relationship of the motor, so that the brushless DC motor can generate continuous torque and drive the equipment.

This paper combines the neural network fuzzy PID control to construct a brushless DC motor control system to improve the control effect of the brushless DC motor.

2. Related work

Motor is an important device for energy conversion, and it is indispensable in national production and life. Due to the many advantages of the DC brushless motor, it has received attention from all over the world since it appeared, so it has developed rapidly [1]. So far, its related drive and traditional control technology has been developed relatively mature [2].

People's research on brushless DC motor is popular in the field of brushless DC motor controller, the field of torque ripple suppression, and the field of position sensorless drive and control. In terms of controllers, people used to use discrete components to form drive circuits through logical relationships. However, due to the complex structure, simple functions and poor reliability of such controllers, they have been replaced by dedicated control circuits, single-chip microcomputers, and DSPs [3]. There are many manufacturers of special control chips for brushless DC motors on the market. The more common ones in the market are Motorola, Philips, Toshiba, Hitachi, Sanyo, etc. There are many product models, including those with position sensors and those without position sensors. The peripheral circuit of this control chip is more stable, reliable, powerful and cost-effective than discrete components. However, due to the limitation of its own structure, its function is difficult to expand, and its application is greatly limited. It is often used in low-control requirements. occasion [4]. If considering the flexibility of control and the expansion of some functions in the future, smart chips are often used as the control core of brushless DC motors. Due to the improvement of brushless motor control requirements and the reduction of chip cost, the control chip has been expanded from the original 51 series to various types of microcontrollers with more powerful performance from different companies and models [5]. Due to the increasing demand for brushless DC motors, there have been single-chip microcomputers specially designed for brushless DC motor control systems, which greatly reduces the complexity of control software writing [6]. For occasions with higher control requirements, although the cost of using a single-chip microcomputer is lower, due to the requirements for speed and processing information, the single-chip microcomputer is difficult to perform. Due to the particularity of its internal structure, DSP makes its processing speed very high, which can meet the hardware requirements of complex algorithms [7]. Its product model is rich, and the peripheral circuits of different functions are integrated into one, which has extremely high practicability and reliability. Its internal code security module prevents unauthorized access to internal codes and protects intellectual property. In the field of suppressing torque ripple, the brushless DC motor will generate torque ripple during operation, which will affect the control accuracy of the motor. In severe cases, it will also cause motor resonance and noise, which will affect the reliability of the motor [8]. The stator winding of the brushless DC motor has cogging. When the motor rotates, due to the interaction of the rotor permanent magnet magnetic field and the stator electromagnetic field, it will be affected by an unbalanced torque in the torque direction. By inclining the motor cogging by 10°; changing the distribution of the windings under each pole to make it asymmetrical to increase the fundamental frequency; improving the influence of the cogging opening by some materials with good magnetic permeability. When controlling the operation of the brushless DC motor, the added armature current is designed according to the ideal trapezoidal wave of the stator winding back EMF [9]. However, when the motor is running, the back EMF of the stator winding is not an ideal trapezoidal wave, and electromagnetic torque ripple will be formed. One method is to improve the motor structure so that the back EMF is closer to the ideal trapezoidal wave, and the other is to reduce the influence of the back EMF through the stator current by detecting the back EMF. This method has high requirements on measurement, and offline detection is often used [10]. Due to the inductance of the brushless DC motor, a delay occurs during commutation. The main torque ripple of the brushless DC motor comes from the commutation of the switching circuit, and the commutation strategy can be changed to suppress the torque ripple by overlapping commutation, hysteresis current, PWM chopping and other methods [11]. Due to the complexity of BLDC motors, it is difficult to describe them using precise mathematical methods. Due to the emergence of modern control technologies such as fuzzy control and neural network, and high-performance processing chips, there has also been an application of estimating the motor torque according to modern control theory and comparing it with the specified value to suppress torque ripple by adjusting the

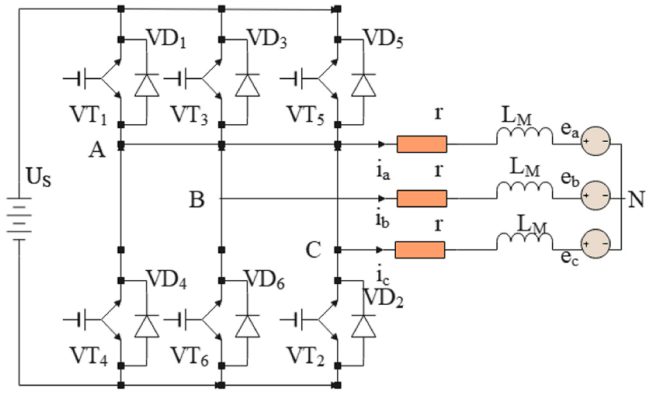

Fig. 1. The working principle diagram of the BLDCM control system.

current [12]. Because there are many reasons for the formation of torque fluctuations of brushless DC motors, it is difficult to accurately analyze the generation mechanism. Various compensation schemes can only be based on specific situations and have certain limitations. A scheme to completely eliminate the torque pulsation [13]. The brushless DC motor drive is usually driven according to the rotor position signal, that is, a brushless DC motor with a position sensor. There is also a method to calculate the stator position to drive the brushless DC motor through the voltage and current signals generated when the motor is running, which is called the position sensorless driving of the DC brushless motor [14]. The research focus of driving a position sensorless DC brushless motor is to accurately sense the position of the motor rotor. Some detect the motor position according to the principle that the current and the rotation speed of the motor rotor are kept constant when the motor stator drives the motor rotor when the motor rotates [15], and some methods detect the voltage across the freewheeling diode of the motor MOSFET in parallel when the motor rotates. to judge the motor position [16].

3. Brushless DC motor control system

3.1. Basic principle of brushless DC motor and pulsation analysis of torque

The BLDCM drive control system mainly includes a Hall position sensor, a brushless DC motor body, an electronic switch module, and a signal control module.

U_S is the bus voltage at which the brushless DC motor operates. Each transistor of VT_1 to VT_6 corresponds to each freewheeling diode of VD_1 to VD_6 to form the control circuit of the BLDCM; the three L_M respectively correspond to the three-phase stator windings of the BLDCM, and they are star-connected in this schematic diagram. The working principle diagram of its circuit is shown in Fig. 1.

Fig. 2 is a schematic diagram of the rotation angle of the rotor and the resultant magnetic field after the 6 transistors of the inverter bridge in the motor control system are turned on in a 360 electrical cycle. When the rotor of the motor rotates by 60 electrical degrees, the three-phase stator windings of the motor will switch on according to a certain logic. The power-on sequence is ab-phase, ac-phase, be-phase, ba-phase, ca-phase, cb-phase, and the corresponding transistor conduction sequence is: VT6VT1, VT1VT2, VT2VT3, VT3VT4, VT4VT5, VT5VT6.

The waveforms of phase current and back EMF are shown in Fig. 3.

For any one-phase star winding, the voltage formula is as follows:

$$\begin{bmatrix} u_a \\ u_b \\ u_c \end{bmatrix} = \begin{bmatrix} r & 0 & 0 \\ 0 & r & 0 \\ 0 & 0 & r \end{bmatrix} \begin{bmatrix} i_a \\ i_b \\ i_c \end{bmatrix} + \begin{bmatrix} L & M & M \\ M & L & M \\ M & M & L \end{bmatrix} \frac{d}{dt} \begin{bmatrix} i_a \\ i_b \\ i_c \end{bmatrix} + \begin{bmatrix} e_a \\ e_b \\ e_c \end{bmatrix} \tag{1}$$

Since the three-phase windings of the stator are connected in a star, and there is no neutral line in the star connection, according to this, there are:

$$i_a + i_b + i_c = 0 \tag{2}$$

Therefore, $Mi_a + Mi_b + Mi_c = 0$ can be obtained, and after substituting the above formula (1), the voltage formula can be known as:

$$\begin{bmatrix} u_a \\ u_b \\ u_c \end{bmatrix} = \begin{bmatrix} r & 0 & 0 \\ 0 & r & 0 \\ 0 & 0 & r \end{bmatrix} \begin{bmatrix} i_a \\ i_b \\ i_c \end{bmatrix} + \begin{bmatrix} L-M & M & M \\ M & L-M & M \\ M & M & L-M \end{bmatrix} \frac{d}{dt} \begin{bmatrix} i_a \\ i_b \\ i_c \end{bmatrix} + \begin{bmatrix} e_a \\ e_b \\ e_c \end{bmatrix} \tag{3}$$

The torque generated by the motor stator is shown in formula (4):

$$T_e = \frac{P}{\Omega} = \frac{e_a i_a + e_b i_b + e_c i_c}{\Omega} \tag{4}$$

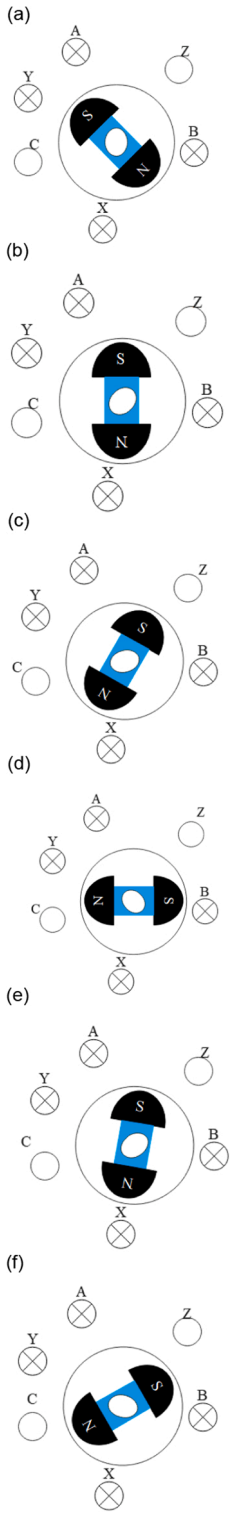

Fig. 2. Working principle of BLDCM.

Because the working mode of the power conversion module of the motor is to conduct two-by-two, the back electromotive force e and the current i_d of the two-phase windings are equal in magnitude and opposite in direction at each moment, while the current of the remaining windings is 0. Therefore, the torque formula of the motor can be simplified to formula (5).

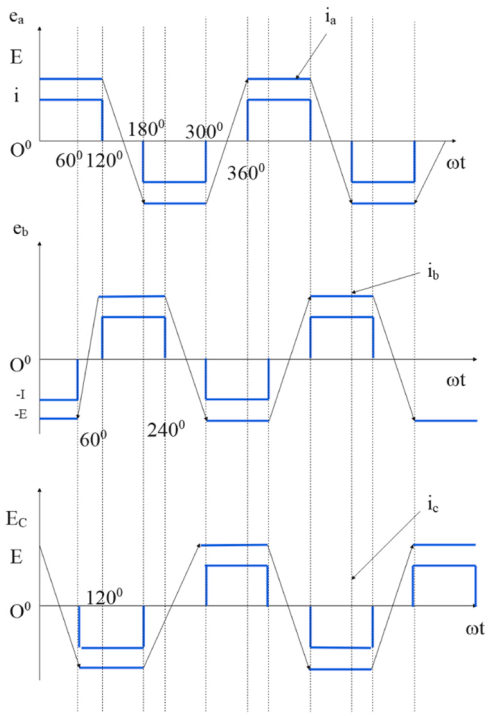

Fig. 3. Current and Induced Potential Waveforms.

Table 1
Current sampling options.

Rotor location	Hall signal (ABC)	Sample phase	Sign relationship with given value	Open phase	Turn off phase
1	101	B	+	A	C
2	100	A	–	C	B
3	110	C	+	B	A
4	010	B	–	A	C
5	011	A	+	C	B
6	001	C	–	B	A

$$T_e = \frac{2EI}{\Omega} \tag{5}$$

In the formula, E and I represent the magnitude of the opposite electromotive force of the motor and the magnitude of the phase current, respectively. According to the mechanical motion formula of BLDCM, we can get:

$$J\frac{d\omega}{dt} = -B\omega + P(T_e - T_L) \tag{6}$$

In the formula, B, J, T_L represent the viscous damping coefficient of the motor, the moment of inertia of the system and the load torque, respectively.

As shown in Table 1, when the rotor position is 1, during the commutation process of the BLDCM, the C-phase current will gradually decrease, and the B-phase current will gradually increase. Therefore, the phase currents of these two phases cannot be used as feedback values to represent the actual working conditions of the current loop [17]. Therefore, this paper adopts the scheme of sampling and controlling the current of the continuous conduction phase, and selects the current Hall sensor with reasonable parameters.

3.2. Analysis of commutation torque ripple of brushless DC motor

As shown in Fig. 4, taking the switch from A^+B^- conduction to A^+C^- conduction as an example, T6 is pulse width modulated before commutation. When T2 is turned on, the current flows through T1 and T6 to form a loop. When T6 is turned off, the B-phase current flows through D3 for freewheeling, and forms a loop with T1. We assume that the power tube and diode are regarded as ideal devices to analyze the commutation torque ripple.

The back EMF of BLDCM is a trapezoidal wave of 120. Ideally, the currents in the three phases of the motor are square waves, as

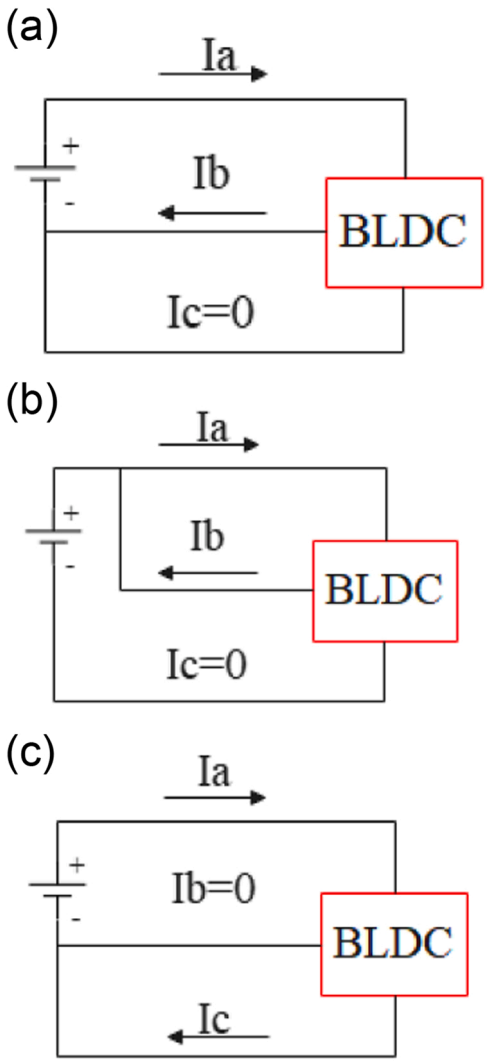

Fig. 4. Simplified diagram of A^+B^- conduction switching to A^+C^- conduction.

shown in Fig. 5a). However, during the commutation process, the rising slope of the ON phase is not equal to the falling slope of the OFF phase [18], which is caused by the existence of the winding inductance of the BLDC motor. During commutation, the current of the non-commutated winding changes, as shown in Fig. 5c), d). In some cases, the rising slope of the on-phase during commutation is equal to the falling slope of the off-phase, as shown in Fig. 5b).

We assume that the back EMF E of phase B does not change during commutation. During the commutation process, the three opposite electromotive forces of A, B, and C are obtained:

$$e_b = e_c = -e_a = E \tag{7}$$

From formula (2), formula (4), formula (7), we get:

$$T_e = \frac{2|I_a|E}{\Omega} \tag{8}$$

In the formula, T_e, E, Ω represent the rotor torque, constant back EMF and rotor mechanical angular velocity of the motor, respectively.

3.3. Implementation of BLDCM current prediction algorithm

Since the commutation torque ripple of BLDCM occurs when the power switching device is commutating, this paper uses the MPC controller for the current loop by analyzing the current model during the commutation period and the non-commutation period [19], as shown in Fig. 6. The current prediction model is selected in real time by the rotor position, and the phase current that needs to be

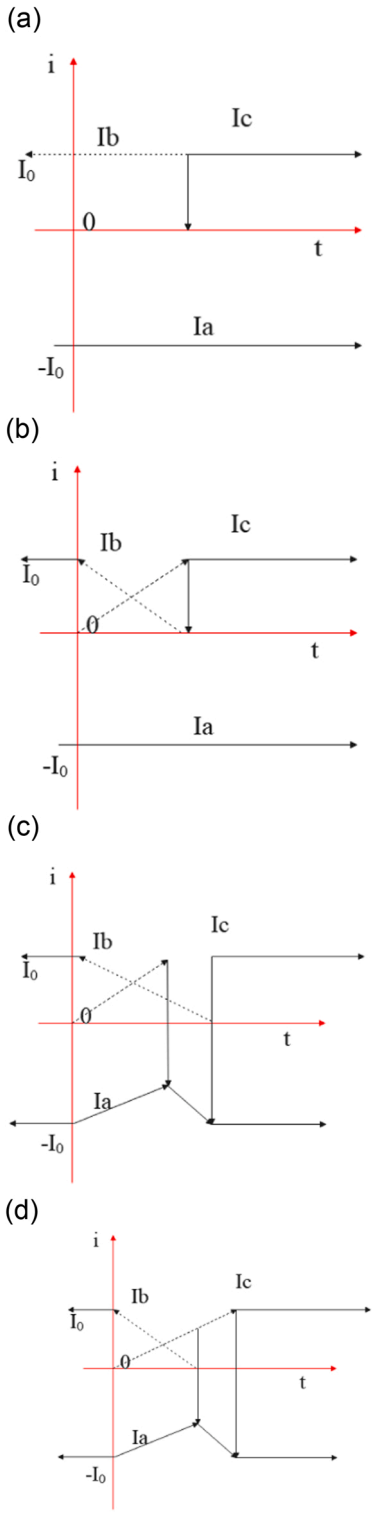

Fig. 5. The waveforms of commutation current under various conditions.

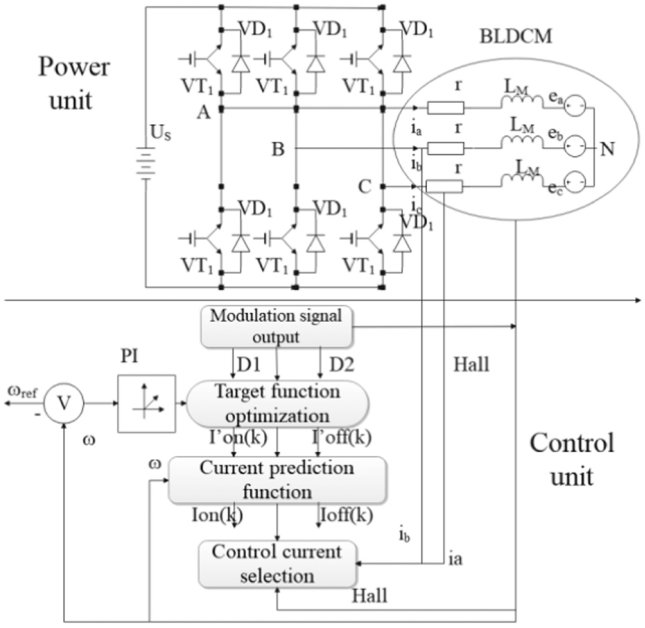

Fig. 6. Block diagram of the brushless DC control system based on model prediction.

Table 2
Pulse width output table of MPC controller during non-commutation period.

$F_0(0)$	$F_0(1)$	Min(g)	D(K)
≥0	≥0	$F_0(1)$	1
>0	<0	0	K
≤0	≤0	$-F_0(0)$	0

controlled is stably controlled, and the purpose is to reduce the commutation torque ripple.

Taking the conduction time of A^+B^- as an example, at this moment $i_c = 0$, it can be obtained from formulas (1) and (2):

$$\begin{cases} H_a - H_b = D_0 U_d \\ i_a = -i_b \end{cases} \tag{9}$$

In the formula, $H_x = L\frac{di_x}{dt} + ri_x + e_x, \mathrm{x} = \mathrm{a},\ \mathrm{b},\ \mathrm{c},\ D_0$ is the modulation duty cycle.

According to formulas (9) and (7), the B-phase current can be solved to satisfy:

$$i_a(t) = e^{-\frac{r}{L}t} I_o + \left(1 - e^{-\frac{r}{L}t}\right) \frac{D_0 U_d - 2E}{2r} \tag{10}$$

In the formula, E and I_o are the opposite electromotive force and the current value at the moment, respectively.

At this moment, we assume that the control period of the current loop is t, $P_t = e^{-\frac{r}{L}t}$ is a constant, and $E(k) = K_e w(k)$. Formula (10) is discretized, and the predicted objective function of the control phase current obtained in the non-commutation stage is obtained as:

$$i_{con}\left(k+l\right) = P_t I_o(k) + (1 - P_t)\frac{D_0(k)U_d - 2E(k)}{2r} \tag{11}$$

Taking the continuous conduction phase current as the control target, according to Table 2, the current value at this time is consistent with the sign direction of the reference value, and the cost function is established to obtain:

$$g = \left|i_a^{'} - i_a(k+1)\right| \tag{12}$$

According to formula (11), it can be known that the predicted current obtained according to the current prediction model has a linear relationship with the duty cycle of the modulation. Therefore, formula (12) can be simplified to:

$$F_0(D_0) = i_a^{'} - i_a\left(k+1\right) = i_a^{'} - \left[P_t I_o(k) + (1 - P_t)\frac{D_0(k)U_d - 2E(k)}{2r}\right] \tag{13}$$

After arranging formula (14), we can get:

Table 3
Pulse width output table of MPC controller during commutation.

$F_0(0)$	$F_0(1)$	min(g)	D(K)
≥0	≥0	$F_1(2)$	2
> 0	< 0	0	S
≤0	≤0	$-F_1(0)$	0

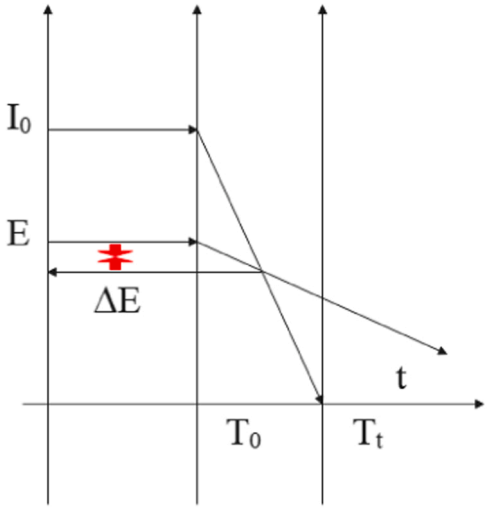

Fig. 7. Turn-off phase current and back EMF waveforms during commutation.

$$K = \frac{2r\left(i_a^{'} - P_t I_o(k)\right)/(1-P_t) + 2E(k)}{U_d} \tag{14}$$

Therefore, during the non-commutation period, the optimal PWM duty ratio predicted by the model is shown in Table 2.

Taking the A^+B^- conduction to C^+B^- conduction as an example, we assume that D_1 is the modulation duty cycle of the on-phase, and D_2 is the modulation duty cycle of the off-phase. Combined with formula (1), we can obtain:

$$\begin{cases} H_a - H_b = D_2 U_d \\ H_c - H_b = D_1 U_d \end{cases} \tag{15}$$

According to formula (15), formula (2) and formula (7), the A-phase current can be solved to satisfy:

$$i_b(t) = e^{-\frac{r}{L}t} I_o - \left(1 - e^{-\frac{r}{L}t}\right) \frac{(D_1 + D_2)U_d - 4E}{3r} \tag{16}$$

In the formula, E and I_o are the opposite electromotive force and the current value at the moment, respectively.

At this moment, we assume that the control period of the current loop is $t, P_t = e^{-\frac{r}{L}t}$ is a constant, and $E(k) = K_e w(k)$, and the formula (16) is discretized to obtain the predicted objective function of the sampled control phase current during the commutation period:

$$i_{con}\left(k+l\right) = P_t I_o(k) - (1-P_t)\frac{(D_1(k) + D_2(k))U_d - 4E(k)}{3r} \tag{17}$$

According to Table 1, the current value at this time is inconsistent with the sign direction of the reference value, and the cost function for establishing the commutation moment is:

$$g = \left|i_b^{'} - i_b(k+1)\right| = \left|i_b^{'} + i_b(k+1)\right| \tag{18}$$

Combined with formula (17), it can be seen that the cost function can be simplified to a function with $(D_1 + D_2)$ as the independent variable. Linear simplification of the cost function, so formula (18) can be obtained:

$$\begin{aligned} &F_1(D_1 + D_2) = i_b^{'} + i_b(k+1) \\ &= i_b^{'} + \left[P_t I_o(k) - (1-P_t)\frac{(D_1(k) + D_2(k))U_d - 4E(k)}{3r}\right] \end{aligned} \tag{19}$$

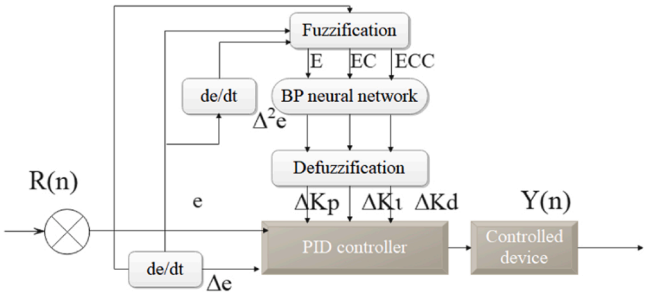

Fig. 8. Fuzzy neural network PID controller structure.

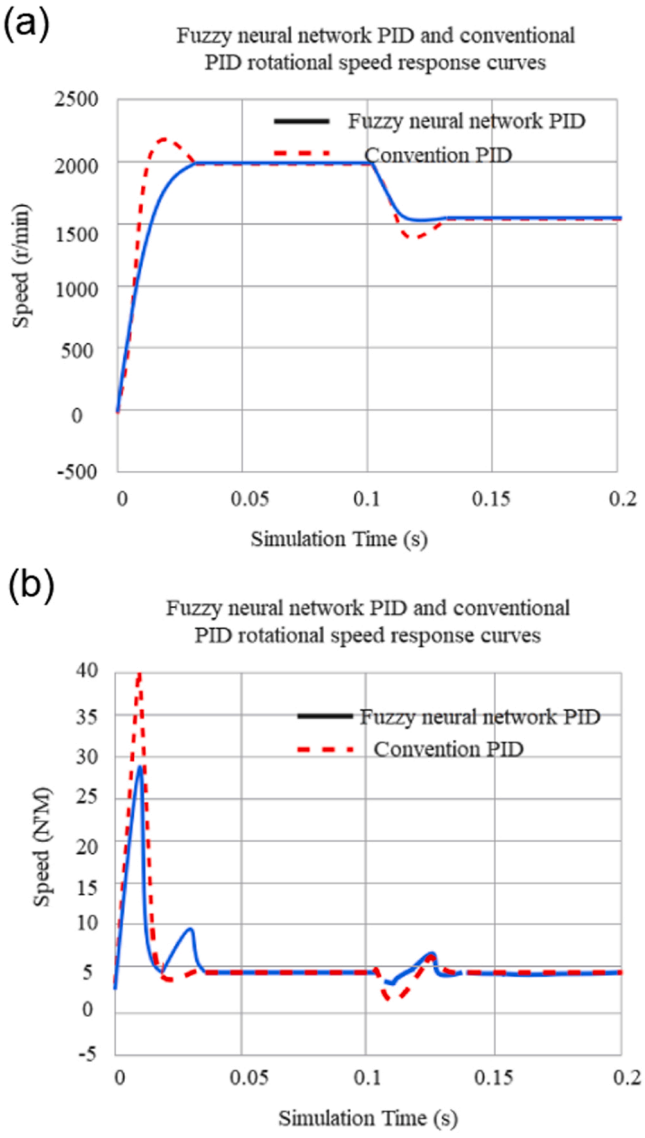

Fig. 9. Response curve of changing rotating speed under no-load condition.

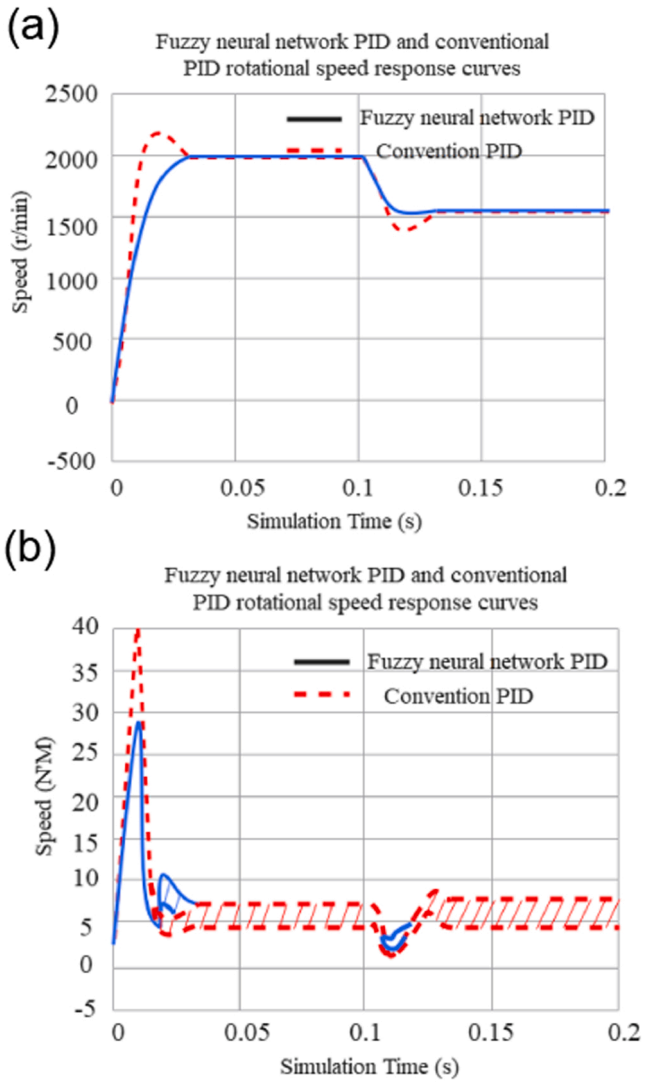

Fig. 10. Response curve of changing rotating speed under load condition.

After finishing formula (13), we can get:

$$D(K) = S = \frac{3r\left(i_b^{'} + P_t I_o(k)\right)/(1 - P_t) + 4E(k)}{U_d} \tag{20}$$

At this time, during the commutation period, the PWM duty ratio predicted by the model is shown in Table 3 below.

However, in the commutation period, the pulse width output of this MPC controller is not optimal, because in the commutation period, the back EMF of the off-phase is also equivalent to E in the formula (17). In the actual commutation process, the back EMF of the off-phase is located on the half waist of the trapezoidal wave, as shown in Fig. 7. The figure shows the equivalent waveform of the off-phase current and the back EMF at the commutation time. The commutation starts at T0 and ends at T1. At this time, the back EMF decreases by E, and the size of E is also related to the rate of the off-phase current and the speed of the motor, that is, the rate of the corresponding off-phase back EMF drop.

Combined with formula (1) and formula (15), the current prediction of the off-phase is as follows:

$$i_a\left(k+l\right) = P_t I_o(k) + (1 - P_t)\frac{(2D_2(k) - D_1(k))U_d - 2E(k)}{3r} \tag{21}$$

When the commutation model is about to end, the situation of $|i_{off}(k+1)| < 0$ may occur. Considering the actual control target and object, D_1 and D_2 should be adjusted in real time to make $|ioff(k+1)| = 0$. At this time, in the last modulation of switching, $D_2 = 0$, and in combination with formula (21), D_1 should satisfy the formula as follows:

$$D_1 = \frac{3rP_t i_{off}(k)}{(1-P_t)} - \frac{2E}{U_d} \tag{22}$$

4. Research on brushless DC motor control system based on neural network fuzzy PID control

The structure of the fuzzy neural network PID controller is shown in Fig. 8. The controller is divided into three parts. The first part is the PID controller, which constitutes a double closed-loop control regulator. The second part is fuzzification, which fuzzifies the system error, the change of the error and the change of the error change as the input of the BP neural network. The third part is the BP neural network, which plays the role of fuzzy reasoning. It self-learns according to the input, and defuzzifies the output, and continuously adjusts the adjustment values of the three parameters of the PID controller Δkp, Δki, and Δkd to achieve optimal control.

In this paper, MATLAB/SIMULINK is used to simulate the double closed-loop control system of the brushless DC motor. In this paper, simulations are carried out under no-load and load conditions, respectively, and the speed response and torque curves of the brushless DC motor (BLDCM) control system are obtained as shown in Figs. 9 and 10. At the same time, the system simulation results of the conventional PID controller are used as a comparison.

From the simulation results, it is not difficult to see that the system based on fuzzy neural network PID has zero speed overshoot when starting under no-load and load conditions, and the adjustment time and starting torque fluctuation are significantly smaller than those of the system based on conventional PID.

5. Conclusion

In order to improve the accuracy of the brushless DC motor control system and accurately demonstrate the influence of the control algorithm on the control accuracy, it is necessary to accurately establish the ontology model of the brushless DC motor, which is an important part of the entire system and the premise of accurately studying the control system. In this paper, the brushless stagnation motor control system structure based on neural network fuzzy PID control is designed, and the current adopts the double closed-loop control system of current hysteresis control. Moreover, this paper introduces the mathematical model, fuzzy control and neural network control of the motor and its algorithm. At the same time, based on the control system, the simulation model of brushless DC motor control system is established in MATLAB, and the simulation experiment is carried out. The simulation results show that the brushless DC motor control system based on neural network fuzzy PID control can effectively improve the control effect.

Declaration of Competing Interest

The authors declare that they have no known competing financial interests or personal relationships that could have appeared to influence the work reported in this paper.

Data Availability

No data was used for the research described in the article.

Acknowledgements

This work was supported by Key projects of Natural Science Foundation of Shandong Province in 2020 [ZR2020KC008]; Research and innovation team of Binzhou University:Research and innovation team of aviation intelligent control and special motor; Binzhou Key Laboratory: Binzhou Key Laboratory of electric drive.

References

[1] E. Artigao, A. Honrubia-Escribano, E. Gómez-Lázaro, In-service wind turbine DFIG diagnosis using current signature analysis, IEEE Trans. Ind. Electron. 67 (3) (2019) 2262–2271.
[2] N. Bushra, Hassan F. Alsunbuli, Widad Fakhruldeen, Nor M. Ismail, Mahyuddin, Hybrid beamforming with relay and dual-base stations blockage mitigation in millimetre-wave 5G communication applied in (VIOT), Comput. Electr. Eng. 100 (2022), https://doi.org/10.1016/j.compeleceng.2022.107953.
[3] F. Chen, Z. Fu, Z. Yang, Research on intelligent fault identification technology of wind turbine supported by fault knowledge base, AMSE J. -AMSE IIETA Publ. -2017-Ser.: Model. A 90 (1) (2017) 1–15.
[4] X. Chen, W. Xu, Y. Liu, M.R. Islam, Bearing corrosion failure diagnosis of doubly fed induction generator in wind turbines based on stator current analysis, IEEE Trans. Ind. Electron. 67 (5) (2019) 3419–3430.
[5] F. Cheng, L. Qu, W. Qiao, L. Hao, Enhanced particle filtering for bearing remaining useful life prediction of wind turbine drivetrain gearboxes, IEEE Trans. Ind. Electron. 66 (6) (2018) 4738–4748.
[6] A. Dameshghi, M.H. Refan, Wind turbine gearbox condition monitoring and fault diagnosis based on multi-sensor information fusion of SCADA and DSER-PSO-WRVM method, Int. J. Model. Simul. 39 (1) (2019) 48–72.
[7] A. Dameshghi, M.H. Refan, P. Amiri, Wind turbine doubly fed induction generator rotor electrical asymmetry detection based on an adaptive least mean squares filtering of wavelet transform, Wind Eng. 45 (2) (2021) 138–159.
[8] H. Gu, W.Y. Liu, Q.W. Gao, Y. Zhang, A review on wind turbines gearbox fault diagnosis methods, J. Vibroeng. 23 (1) (2021) 26–43.
[9] A. Hameed Al-ali, L. Khalid Qalaja, A. Abu-Rumman, M. Ratajczak-Mrozek, Justice in organizations and its impact on Organizational Citizenship Behaviors: a multidimensional approach, Cogent Bus. Manag. 6 (2020) 1.
[10] Z. Hashemi, A. Rahideh, Rotor electrical fault detection of wind turbine induction generators using an unscented Kalman filter, Iran. J. Sci. Technol., Trans. Electr. Eng. 44 (2) (2020) 979–988.

[11] A. Hu, L. Xiang, L. Zhu, An engineering condition indicator for condition monitoring of wind turbine bearings, Wind Energy 23 (2) (2020) 207–219.
[12] H.J. Mohammed, A.T. Naiyf, A.J. Thaer, S.K. Khbalah, Assessment of sustainable renewable energy technologies using analytic hierarchy process, in: IOP Conference Series: Earth and Environmental Science, vol. 779, IOP Publishing, 2021, 012038 (June).
[13] A.R. Nejad, P.F. Odgaard, T. Moan, Conceptual study of a gearbox fault detection method applied on a 5–MW spar-type floating wind turbine, Wind Energy 21 (11) (2018) 1064–1075.
[14] P. Qian, X. Ma, P. Cross, Integrated data-driven model-based approach to condition monitoring of the wind turbine gearbox, IET Renew. Power Gener. 11 (9) (2017) 1177–1185.
[15] W. Qiao, L. Qu, Prognostic condition monitoring for wind turbine drivetrains via generator current analysis, Chin. J. Electr. Eng. 4 (3) (2018) 80–89.
[16] X. Sheng, S. Wan, L. Cheng, Y. Li, Blade aerodynamic asymmetry fault analysis and diagnosis of wind turbines with doubly fed induction generator, J. Mech. Sci. Technol. 31 (10) (2017) 5011–5020.
[17] X. Wang, W.Y. Liu, Y. Zhang, H. Gu, A novel wind turbine fault diagnosis method based on generator current analysis, J. Vibroeng. 22 (8) (2020) 1758–1769.
[18] S. Wei, X. Zhang, Y. Xu, Y. Fu, Z. Ren, F. Li, Extended Park's vector method in early inter-turn short circuit fault detection for the stator windings of offshore wind doubly-fed induction generators, IET Gener., Transm. Distrib. 14 (18) (2020) 3905–3912.
[19] L. Zhao, Y. Zhou, I.B. Matsuo, S.K. Korkua, W.J. Lee, The design of a remote online holistic monitoring system for a wind turbine, IEEE Trans. Ind. Appl. 56 (1) (2019) 14–21.

Ran Zhang, Doctor of Electrical Engineering, Lecturer. Graduated from the Shandong University in 2011. Worked in Binzhou university.His research interests include control and simulation of electrical machine，more than20 papers published and 1 book published.

Lianxue Gao, associate professor in the school of electrical engineering of Binzhou University. He graduated from Shandong university, China. Now he is vice dean of the school of electrical engineering. His mainly research is focused on the motor intelligent controlling and energy saving. He has published more than 10 papers on the research of brushless DC motors.